ADVANCED ENERGY MATERIALS
www.advenergymat.de

Efficient Electro-Catalysts for Enhancing Surface Activity and Stability of SOFC Cathodes

*Dong Ding, Mingfei Liu, Zhangbo Liu, Xiaxi Li, Kevin Blinn, Xingbao Zhu, and Meilin Liu**

The search for a sustainable supply of clean and economical energy has stimulated great interest in fuel cells for direct conversion of chemical fuels to electricity. Among all types of fuel cells, solid oxide fuel cells (SOFCs) are the cleanest and most efficient ones with excellent fuel flexibility. They are capable of direct utilization of a wide variety of fuels, from hydrogen to hydrocarbons, coal gas, and bio-derived fuels.[1–4] One of the technical hurdles to commercialization of SOFC technologies, however, is the high operating temperature that requires the use of expensive materials.[5–7] The enhancement of cathode activity represents a vital step toward successful reduction in operating temperature since the resistance to oxygen reduction reaction (ORR) contributes the most to energy loss in the existing SOFCs, more so at lower temperatures.[8]

A good SOFC cathode material must have both fast oxygen exchange kinetics and high mixed ionic-electronic conductivity. To date, various cathode materials have been studied, including $La_{1-x}Sr_xMnO_{3-\delta}$ (LSM),[9] $La_{0.6}Sr_{0.4}Co_{0.2}Fe_{0.8}O_{3-\delta}$ (LSCF),[10] $Sm_{0.5}Sr_{0.5}CoO_{3-\delta}$ (SSC),[11] $Ba_{0.5}Sr_{0.5}Co_{0.8}Fe_{0.2}O_{3-\delta}$ (BSCF),[12] $PrBaCo_2O_{5+\delta}$ (PBC),[13] and their derivatives.[14–18] Although some of these cathode materials show high ORR activity at low temperatures, their long-term stability and compatibility with electrolyte and/or other cell components, especially at high temperatures required for fabrication, limit their application in SOFCs.[19] As a result, the state-of-the-art cathode materials are still based on LSM (>800 °C) and LSCF (<800 °C). The performance of an LSM cathode is limited often by its low oxygen ion conductivity at low temperatures, which diminishes the effective width of the three-phase boundaries (TPBs) or the active sites for ORR. An LSCF cathode, on the other hand, may suffer from low surface activity for ORR[20,21] and inadequate long-term durability,[22] which may correlate strongly with the change in surface chemistry, structure, and morphology of LSCF under service conditions.[22] To overcome these issues, a solution infiltration process has been introduced to coat the surface of LSCF with a chemically stable and electro-catalytically active material.[23–26] In a catalyst-infiltrated LSCF cathode, the porous LSCF backbone serves as a "highway" for facile transport of both oxygen ions and electronic defects because of its excellent ambipolar conductivity, while the catalyst coating modifies the LSCF surface to offer higher electro-catalytic activity and greater stability. In our previous studies, discontinuous coatings of SSC,[23] $La_{0.4875}Ca_{0.0125}Ce_{0.5}O_{2-\delta}$ (LCC)[24] and $Ce_{0.8}Sm_{0.2}O_{1.9}$ (SDC)[25] were found efficient in reducing polarization resistance to ORR. Meanwhile, a conformal thin-film coating of LSM enhanced both surface ORR activity and the stability of LSCF cathodes.[26] While the concept feasibility of surface modification has been demonstrated, the degree of performance improvement can be further enhanced.

In this article, we report our findings in modification of an LSCF cathode using new electro-catalysts with higher ORR activity and better chemical stability: $Pr_{0.75}Sr_{0.2}MnO_{3-\delta}$ (PSM) and $PrSrCoMnO_{6-\delta}$ (PSCM), including the interfacial polarization resistance (R_p), long term stability, and cathodic activation behavior of PSM- and PSCM-infiltrated LSCF cathodes under typical SOFC operating conditions. Both PSM and PSCM are derivatives of a doped lanthanide manganite, a family of cathode materials that has been widely studied for SOFC. The similarity in crystal structure of PSM and PSCM to that of LSCF (perovskite) allows for facile formation of a conformal coating of them on an LSCF surface, which has the potential to suppress SrO segregation or enrichment on the surface, thus enhancing stability and durability under operating conditions.[27] The choice of Pr in the A site was inspired by the superior oxygen exchange activity of this element in the $Ln_{1-x}Sr_xMnO_{3-\delta}$ and $LnSrCoMnO_{6-\delta}$ family of materials (where Ln represents the lanthanide elements from Ln to Gd).[28–30] Perovskite cathodes with Mn in the B-site are known for their stability over long term operation while cobaltites show excellent ionic and electronic conductivities.[31] The aim of substituting cobalt in the B site of the lanthanide manganite is to increase the catalytic activity without compromising the stability.

In order to determine the phase composition of the catalysts coated on an LSCF cathode, PSCM and PSM powders were derived from the same solution used for solution coating. The X-ray diffraction (XRD) patterns (in **Figure** 1a and Figure SI1) indicate that PSM and PSCM (calcined at 900 °C for 1 h) have a simple and complex perovskite phase, respectively. A structural model for PSCM (Figure 1b) is proposed based on the estimated lattice parameters (Table SI1). The Mn and Co ions (the B cations) are randomly distributed at the center of the BO_6 octahedrons. The Pr and Sr ions (the A cations) are at the center of the layers surrounded by tilted BO_6 octahedrons. The chemical compatibilities between PSM, PSCM, and LSCF under actual synthesis conditions were also investigated. The mixtures were obtained by dispersing LSCF powders in the PSM and the PSCM solution, followed by drying and annealing the resulting powder mixtures at 900 °C in air for 500 hours.

Dr. D. Ding, Dr. M. F. Liu, Z. B. Liu,
X. X. Li, K. Blinn, X. B. Zhu, Prof. M. Liu
Center for Innovative Fuel Cell
and Battery Technologies
School of Materials Science and Engineering
Georgia Institute of Technology
Atlanta, GA 30332-0245, USA
E-mail: meilin.liu@mse.gatech.edu

DOI: 10.1002/aenm.201200984

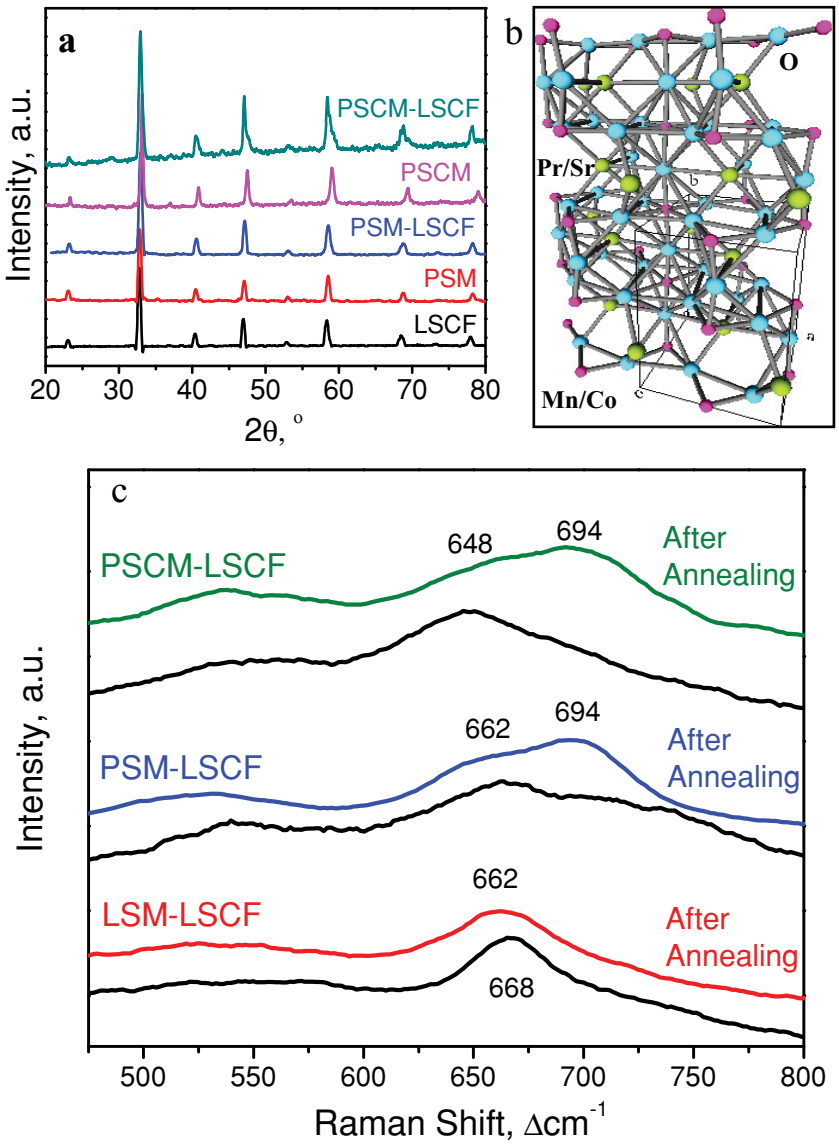

Figure 1. XRD and Raman analysis of the catalysts as well as catalyst-LSCF mixtures: (a) XRD patterns of LSCF, PSM, PSCM and the mixtures of them; (b) Proposed crystal structure of PSCM based on Rietveld refinement (The green, pink and blue atoms represent Pr/Sr cation, Mn/Co cation and O anion respectively; Cell distance is shown as doubled along a and b axis.). (c) Raman spectra collected in air from LSM-LSCF, PSM-LSCF, and PSCM-LSCF samples before and after annealing in air at 1000 °C for 100 hours.

There was no evidence of any secondary phases in the XRD patterns for either case, suggesting that PSM and PSCM both have excellent phase stability against LSCF under the conditions studied.

Possible chemical interdiffusion between the PSM/PSCM catalysts and LSCF substrate were further investigated by annealing the powder mixstures at 1000 °C in air for 100 hours and analyzing the resulting products using Raman spectroscopy. Figure 1c shows parts of Raman spectra collected from LSM-LSCF, PSM-LSCF, and PSCM-LSCF mixture samples before and after annealing. In each of the samples, the broad set of Raman bands between 600 and 750 cm^{-1} correspond to vibrations involving the B ions and oxygen ions in the bulk material.[32] In the LSM-LSCF spectrum, this band is nearly symmetric in character. After annealing, the band retained its shape but its center shifts slightly from 668 to 662 cm^{-1}, corresponding likely to some exchange of Mn, Co, and Fe ions in the bulk material during the course of the annealing. Similar inter-exchange was observed in LSM-coated LSCF samples, where an "LSMCF" inter-phase was formed between LSM and LSCF.[26] In the PSM-LSCF and PSCM-LSCF spectra before annealing, the left side of this band was slightly more prominent. After annealing, however, the right shoulder of the band (694 cm^{-1}) became more pronounced, indicating a greater distortion in the lattice than in the LSM-LSCF case that was due likely to changes in the A-site ions. In similar materials, this Raman band changed similarly when different ions were doped in the A-site.[32] Therefore, in the PSM-LSCF and PSCM-LSCF cases, some inter-exchange likely took place between the Pr, La, and Sr ions, likely leading to the formation of a "LPSMCF" perovskite phase. However, there was no evidence in the Raman analysis that might suggest the formation of any undesirable, non-perovskite secondary phase.

Figure 2a and 2b shows the typical surface morphologies of a blank LSCF surface and a PSCM coated LSCF surface. Grains of the blank LSCF are very smooth with clear triple junctions. With PSCM coating, the continuous and dense film is visible on the surface of LSCF grains, making it appear rougher and very different from the typical microstructures of particle-coated cathode surface.[33–36] It is also noted that there is clear contrast across different grains due possibly to the differences in orientation of the PSCM films inherited from the underlying LSCF grains. When these catalysts were coated on the surface of a porous LSCF cathode through a solution infiltration process, they appear similar (Figure 2c and 2d). The thickness of the thin-film coating was estimated from the following equation:

$$L = \frac{VCM}{\rho S} \quad (1)$$

where V is the volume of the solution, C is the solution concentration, M is the molar weight of the catalyst used for coating, ρ is the theoretical density of the infiltration material, and S is the inner surface area of porous cathode that was coated with the solution. When V, C, and S were held constant, the thickness L is determined mainly by the ratio of M/ρ, which is similar for LSM, PSM, and PSCM (varied from 35 to 37 mol cm^3 g^{-2}). Therefore, it is reasonable to assume that the thicknesses of the

Adv. Energy Mater. 2013,
DOI: 10.1002/aenm.201200984

PSM and PSCM coatings are comparable to that of the LSM coating on LSCF, which was determined to be in the range of 2 to 23 nm by careful TEM analysis.[26]

The electrochemical behavior of the catalyst-infiltrated LSCF cathodes was characterized at 750 °C under open circuit conditions using impedance spectroscopy (**Figure 3**a). Unlike the LSM-infiltrated LSCF cathode, which had higher impedance than the blank LSCF cathode, the PSM-infiltrated LSCF cathode displayed smaller impedance than the blank LSCF cathode. Clearly, the PSM-infiltrated LSCF has higher catalytic activity for ORR than the LSM-infiltrated LSCF cathodes. The PSM coating significantly reduced the interfacial polarization resistance (R_p) of the LSCF cathode even under open-circuit voltage (OCV) condition in contrast to the LSM infiltration. The PSCM infiltration further decreased R_p at the same concentration of infiltration. For example, R_p was 0.107 and 0.093 Ω cm^{-2} for the PSM and PSCM infiltrated LSCF cathodes, contrasting with the 0.126 and 0.197 Ω cm^{-2} for the blank LSCF and LSM infiltrated LSCF cathodes at 750 °C. Figure 3b shows the temperature dependence of R_p for these catalyst-infiltrated LSCF cathodes. At an intermediate temperature range, the PSCM infiltration provided the lowest R_p among these Mn-containing catalysts. All of the curves appear to have similar slopes, indicating that the primary ORR mechanism remains the same. We employed symmetrical cells with a three-electrode configuration to evaluate the polarization behavior. Unlike LSM infiltration, the PSM and PSCM infiltrated LSCF cathodes initially showed lower R_p compared to blank LSCF cathodes (Figure 3c), followed by a fast reduction in R_p at a given cathodic overpotential, which is likely associated with the higher electrocatalytic activity (Figure SI3, SI4 and SI5) as well as stronger activation behavior (Figure SI6) for PSM and PSCM. This suggests that PSM and PSCM infiltration are able to further enhance performance under operation conditions.

Shown in **Figure 4**a is the typical performance of button cells infiltrated with different catalytic coatings and operated at 750 °C under a constant cell voltage of 0.7 V. Within 550 hours, the cells with the PSCM-infiltrated LSCF cathodes showed the best performance with significant activation behavior. Compared to the cells with LSM and PSM infiltration, the PSCM infiltrated cells showed a gradual increase in performance, implying a continuous activation during operation. The "long-term activation" effect could counter against other degradation mechanisms and stablize cell output. This phenomenon has attracted our attention for further study. After over 500 hours of operation, the performance enhancement (compared with that of the cell with a blank LSCF cathode) was 41.6%, 51.5%, and 61.7% for LSM, PSM, and PSCM infiltration, respectively. Due to possible degradation of the blank LSCF cathode during operation, an even larger performance difference would be expected for operation over a longer period of time. The degradation rate of the cell with the blank LSCF cathode in this study was ~0.035% per hour, considerably lower than 0.06% per hour reported by others[21] under similar conditions. The current-voltage characteristics and the corresponding power densities for the cells with or without infiltration are quite different (Figure 4b and 4c). In comparison with the LSM- infiltrated LSCF cathode, PSM- and PSCM-infiltrated LSCF displayed stronger enhancement in activity and stabilitly of full cells, which may be attributed to higher intrinsic electro-catalytic activity, stronger activation, and desirable cation inter-diffusion between infiltrates and LSCF backbone.

In conclusion, both electro-catalytic activity and stability of the-state-of-the art LSCF cathode have been enhanced by more active Mn-based catalyst coatings as demonstrated in symmetrical and anode-supported cells. Further, the infiltration process used to apply the coating is simple and economically feasible for application to commercial cells. First, the catalyst coating is very thin; in fact, an ideal thickness of the Mn-based catalyst coating is only about 10 to 50 nm, far thinner than other cell components such as the anode support (0.3–0.7 mm), electrolyte (10–20 μm), or cathode backbone (50 μm). This implies that other catalytically active materials, such as Pr- or Pd-containing ones, which are too expensive to use as bulk cathode material, may become economically feasible. It is worth pointing out that Pr-containing Mn-based catalysts studied in this work are superior in activity and stability enhancement over LSM. Second, compared with most infiltration cases where multiple steps are needed to increase loading in order to obtain sufficient conductivity for optimal performance, our infiltration process is more efficient (one step), making it possible to be readily implemented in typical SOFC fabrication.

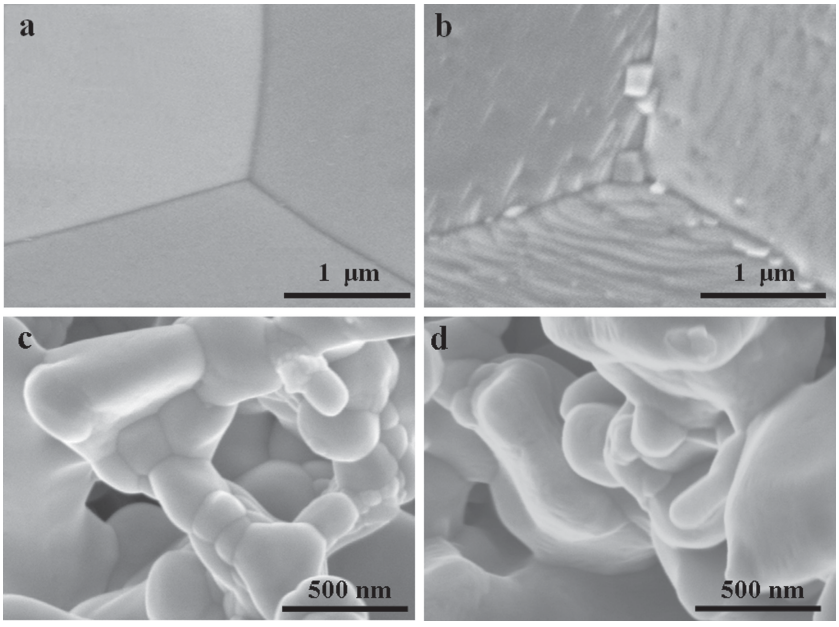

Figure 2. Surface morphology of blank and catalyst-coated LSCF: Typical surface views (SEM images) of (a) an LSCF pellet fired at 1350 °C for 5 hours; (b) a PSCM coated LSCF pellet annealed at 900 °C for 1 hour; (c) a porous LSCF cathode fired at 1080 °C for 2 hours; and (d) a PSCM-coated LSCF cathode fired at 900 °C for 1 hour.

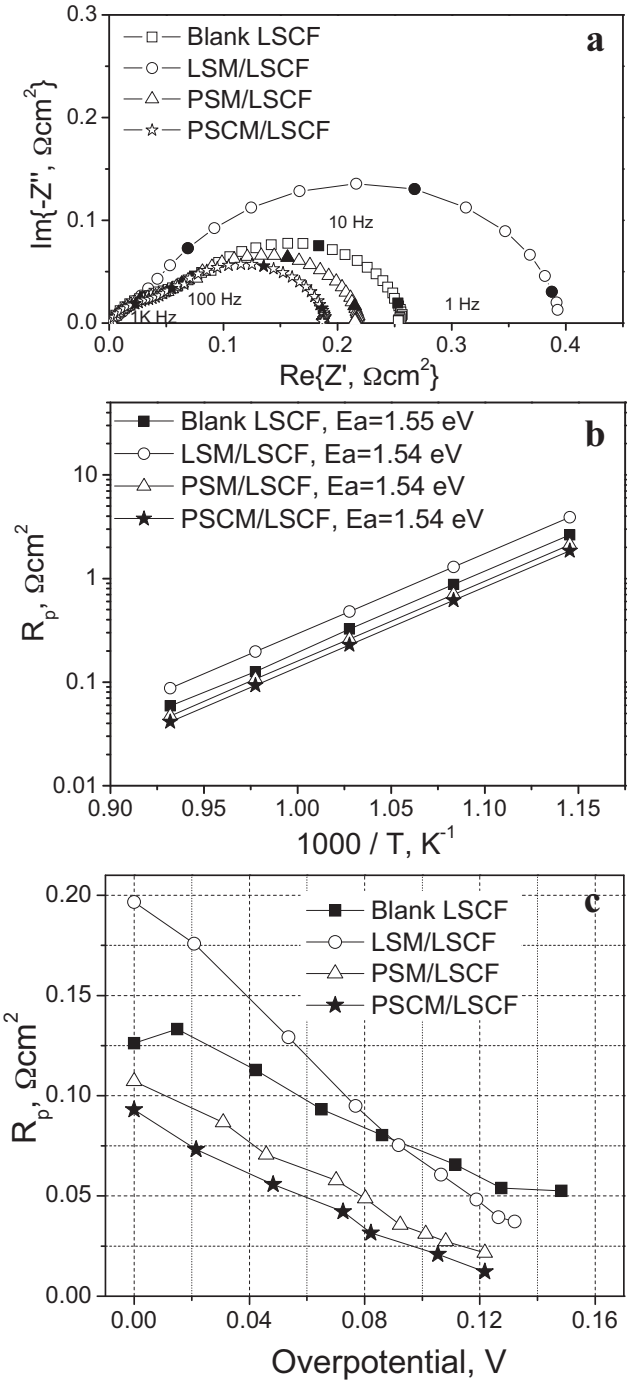

Figure 3. Electrochemical performances of catalyst-infiltrated LSCF cathodes in symmetrical cells: (a) Typical impedance spectra of catalyst-infiltrated LSCF cathodes measured at 750 °C under open circuit (OCV) conditions; (b) Temperature dependence of interfacial polarization resistance (R_p) of catalyst-infiltrated LSCF cathodes under OCV conditions; (**c**) Interfacial polarization resistance (R_p) versus cathodic overpotential (η) for catalyst-infiltrated LSCF cathodes as measured at 750 °C.

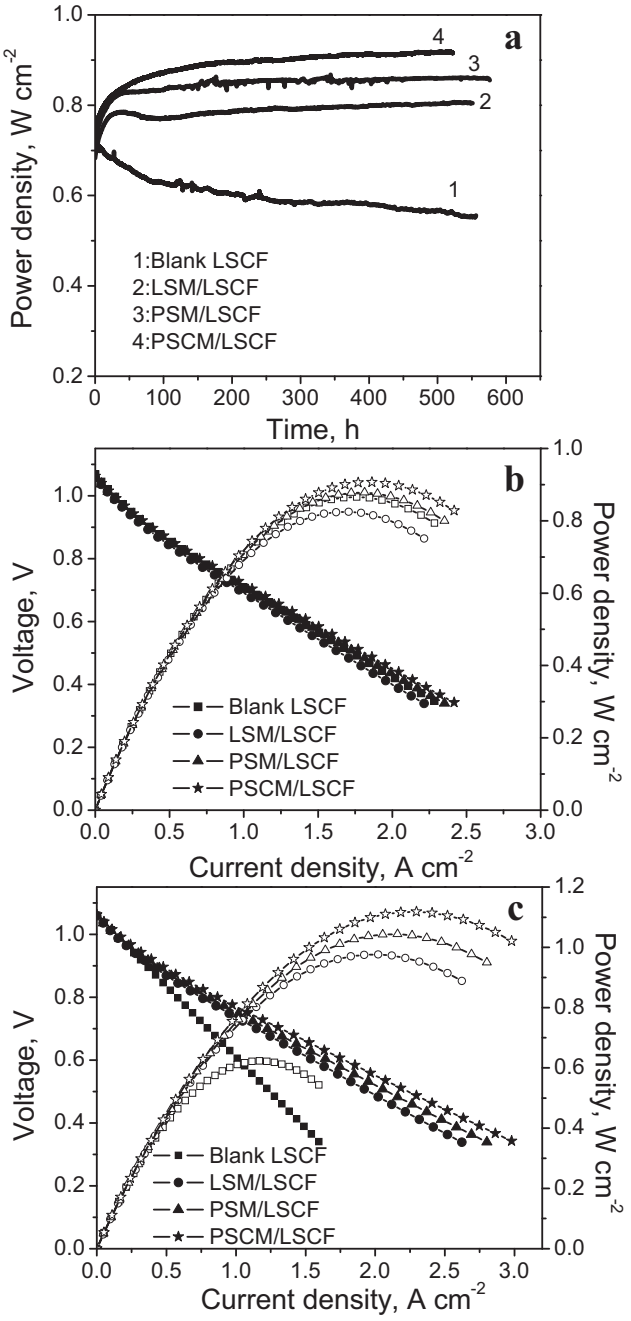

Figure 4. Electrochemical performances of catalyst-infiltrated LSCF cathodes in anode-supported cells. (a) Power outputs of anode-supported cells with catalyst-infiltrated LSCF cathodes at a constant cell voltage of 0.7 V at 750 °C with humidified H_2 (3 vol% water vapor) as the fuel and stationary air as the oxidant; Current-voltage characteristics and the corresponding power densities for the cells with catalyst-infiltrated LSCF cathodes measured at 750 °C (b) before and (c) after operation for over 500 hours.

Experimental Section

Preparation of LSM, PSM, and PSCM Solution for Infiltration: Stoichiometric amounts of high-purity praseodymium nitrate hydrate, lanthanum nitrate hexahydrate, strontium nitrate, cobalt nitrate hexahydrate, and manganese nitrate hydrate (all from Alfa Aesar) were dissolved in a mixture of deionized water and ethanol (at a volume ratio of 1:1) to form 0.1 mol L^{-1} solution. 5 wt.% polyvinyl pyrrolidone (PVP) were added to the solution as a surfactant and a stoichiometric amount

Adv. Energy Mater. **2013**,
DOI: 10.1002/aenm.201200984

of glycine was added as a complexing agent and the fuel for subsequent self-combustion. 5 µL of the stock solution was deposited on the as-prepared LSCF surface or a porous cathode. After overnight drying in ambient air, the resulting coating was fired at 900 °C in air for 1 hour.

Fabrication of Symmetrical Cells and Test Cells with Three-electrode Configurations: YSZ pellets were prepared by uniaxially pressing commercially available YSZ powders (Daiichi Kigenso, Japan) followed by sintering at 1450 °C for 5 h to achieve relative density of ~98%. LSCF (Fuelcell Materials, US) green tapes were prepared by tape-casting, which were then bound onto both sides of a YSZ electrolyte pellet using a slurry of $Sm_{0.2}Ce_{0.8}O_{1.9}$ (SDC, the buffer layer). The cells were then co-fired at 1080 °C for 2 h to form porous LSCF electrodes (with an area of 0.3 cm^2) on YSZ. The SDC powder was synthesized using a chemical co-precipitation process.[37,38] The SDC powder was then dispersed in acetone with V-006A (Heraeus, US) as binder and ball-milled for 24 h to form a stable SDC slurry. The symmetrical cells were also tested in a three-electrode configuration. The LSCF cathode with/without catalyst coating were used as working electrode (WE) and counter electrode (CE), respectively. Pt paste was fired at 900 °C for 1 h as reference electrode (RE) by positioning it as close to working electrode as possible.

Fabrication of Anode-Supported Full Cells: Tape-cast NiO/YSZ anode-support was first fabricated and pre-fired at 850 °C for 2 h. Then, an active NiO/YSZ layer (~15 µm) and a YSZ electrolyte (~15 µm) were sequentially deposited on the anode support by a particle suspension coating process followed by co-firing at 1400 °C for 5 h.[39] The LSCF cathode was then applied to the YSZ electrolyte using the same procedures as described earlier for the fabrication of symmetric cells.

Characterization of Phase composition and Microstructure of Cathode: The phase compositions of LSCF, PSM, and PSCM powders as well as their composites were determined by XRD. LSCF powders were fired at 1080 °C for 2 hours (the same as the fabrication process of the cathode backbone). PSM and PSCM powder precursor were firstly obtained from a glycine-combustion method and were then fired at 900 °C for 1 hour (the same as the fabrication process of their coating), and their composites were obtained by dispersing LSCF powders (1080 °C for 2 hours) in PSM and PSCM solution (powder weight ratio = 50:50) followed by drying in an oven and firing at 900 °C in air for one hour. Raman spectroscopy (Renishaw RM1000) was performed using 514 nm laser excitation on mixed PSM-LSCF and PSCM-LSCF samples after being annealed at 1000 °C for 100 hours for further chemical analysis. The microstructure and morphology of the LSCF pellets with/without catalysts coatings were examined using a scanning electron microscope (SEM, LEO 1530).

Electrochemical Measurements: The area specific resistances (ASR) of cathodes were measured in a two electrode symmetric cell configuration using two pieces of Pt mesh as current collector (without Pt paste to avoid its possible contribution to catalytic activity) at 500–800 °C. Impedance spectra were acquired using a Solartron 1255 HF frequency response analyzer interfaced with an EG&G PAR potentiostat model 273A with an AC amplitude of 10 mV in the frequency range from 100 kHz to 0.1 Hz. The overpotential, η, was calculated using the following equation:

$$\eta = U_{WR} - i R_{ohm} \quad (2)$$

U_{WR} is the potential applied between WE and RE, i is the corresponding current density, and R_{ohm} is the ohmic resistance of the cell. The observed cell current response typically reached a steady state after the DC polarization was applied for ~30 min. To accurately determine the ohmic resistance of the cell, impedance spectra were also collected under identical DC polarization after the cell response was stabilized. The button cells were mounted on an alumina supporting tube for fuel cell testing at 750 °C with humidified hydrogen (3% H_2O) as the fuel and stationary air as the oxidant. The cell performance was monitored with an Arbin multi-channel electrochemical testing system (MSTAT).

Supporting Information

Supporting Information is available from the Wiley Online Library or from the author.

Acknowledgements

This work was supported by the U.S. Department of Energy (DOE) SECA Core Technology Program under Grant No. DENT-0006557 and as part of the Heterogeneous Functional Material (HetroFoaM) center, an Energy Frontier Research Center funded by the U.S. Department of Energy, Office of Science, Office of Basic Energy Science under Award Number DE-SC0001061. DD would like to thank Dr. Mingyang Gong for XRD analysis and discussion.

Received: November 27, 2012
Published online:

[1] N. Q. Minh, *J. Am. Ceram. Soc.* **1993**, *76*, 563.
[2] B. C. H. Steele, A. Heinzel, *Nature* **2001**, *414*, 345.
[3] M. F. Liu, Y. Choi, L. Yang, K. Blinn, W. T. Qin, P. Liu, M. L. Liu, *Nano Energy* **2012**, *1*, 448.
[4] Z. Cheng, J. H. Wang, Y. Choi, L. Yang, M. C. Lin, M. L. Liu, *Energy Environ. Sci.* **2011**, *4*, 4380.
[5] S. C. Singhal, *Solid State Ionics* **2002**, *152*, 405.
[6] L. Yang, S. Z. Wang, K. Blinn, M. F. Liu, Z. Liu, Z. Cheng, M. L. Liu, *Science* **2009**, *326*, 126.
[7] L. Yang, Y. Choi, W. Qin, H. Chen, K. Blinn, M. Liu, P. Liu, J. Bai, T. A. Tyson, M. Liu, *Nat. Commun.* **2011**, *2*, 357.
[8] M. Liu, M. E. Lynch, K. Blinn, F. M. Alamgir, Y. Choi, *Mater. Today* **2011**, *14*, 534.
[9] M. J. L. Ostergard, C. Clausen, C. Bagger, M. Mogensen, *Electrochim. Acta* **1995**, *40*, 1971.
[10] L. W. Tai, M. M. Nasrallah, H. U. Anderson, D. M. Sparlin, S. R. Sehlin, *Solid State Ionics* **1995**, *76*, 273.
[11] C. R. Xia, W. Rauch, F. L. Chen, M. L. Liu, *Solid State Ionics* **2002**, *149*, 11.
[12] Z. P. Shao, S. M. Haile, *Nature* **2004**, *431*, 170.
[13] G. Kim, S. Wang, A. J. Jacobson, L. Reimus, P. Brodersen, C. A. Mims, *J. Mater. Chem.* **2007**, *17*, 2500.
[14] J. W. Kim, A. V. Virkar, K. Z. Fung, K. Mehta, S. C. Singhal, *J. Electrochem. Soc.* **1999**, *146*, 69.
[15] E. P. Murray, M. J. Sever, S. A. Barnett, *Solid State Ionics*, **2002**, *148*, 27.
[16] Y. W. Ju, T. Inagaki, S. Ida, T. Ishihara, *J. Electrochem. Soc.* **2011**, *158*, B825.
[17] D. J. Chen, C. Huang, R. Ran, H. J. Park, C. Kwak, Z. P. Shao, *Electrochem. Commun.* **2011**, *13*, 197.
[18] Q. J. Zhou, F. Wang, Y. Shen, T. M. He, *J. Power Sources* **2010**, *195*, 2174.
[19] C. W. Sun, R. Hui, J. Roller, *J. Solid State Electron.* **2010**, *14*, 1125.
[20] J. A. Lane, S. J. Benson, D. Waller, J. A. Kilner, *Solid State Ionics* **1999**, *121*, 201.
[21] M. Prestat, J. F. Koenig, L. J. Gauckler, *J. Electroceram* **2007**, *18*, 87.
[22] S. P. Simner, M. D. Anderson, M. H. Engelhard, J. W. Stevenson, *Electrochem. Solid State* **2006**, *9*, A478.
[23] X. Y. Lou, S. Z. Wang, Z. Liu, L. Yang, M. L. Liu, *Solid State Ionics* **2009**, *180*, 1285.
[24] M. F. Liu, D. Ding, K. Blinn, X. X. Li, L. F. Nie, M. Liu, *Int. J. Hydrogen Energy* **2012**, *37*, 8613.
[25] L. F. Nie, M. F. Liu, Y. J. Zhang, M. L. Liu, *J. Power Sources* **2010**, *195*, 4704.

[26] M. E. Lynch, L. Yang, W. Qin, J.-J. Choi, M. Liu, K. Blinn, M. Liu, *Energy Environ. Sci.* **2011**, *4*, 2249.
[27] H. Ding, A. V. Virkar, M. Liu, F. Liu, *Phys. Chem. Chem. Phys.* **2013**, *15*, 489.
[28] T. Ishihara, T. Kudo, H. Matsuda, Y. Takita, *J. Electrochem. Soc.* **1995**, *142*, 1519.
[29] T. Ishihara, H. Matsuda, Y. Takita, *J. Am. Chem. Soc.* **1994**, *116*, 3801.
[30] G. C. Kostogloudis, C. Ftikos, *J. Eur. Ceram. Soc.* **2007**, *27*, 273.
[31] C. Sun, R. Hui, J. Roller, *J. Solid State Electrochem.* *14*, 1125.
[32] R. K. Gupta, C. M. Whang, *J. Phys.-Condens. Matter* **2007**, *19*,
[33] S. P. Jiang, W. Wang, *J. Electrochem. Soc.* **2005**, *152*, A1398.
[34] Y. Y. Huang, J. M. Vohs, R. J. Gorte, *J. Electrochem. Soc.* **2005**, *152*, A1347.
[35] T. Z. Sholklapper, C. Lu, C. P. Jacobson, S. J. Visco, L. C. De Jonghe, *Electrochem. Solid State* **2006**, *9*, A376.
[36] Z. Y. Jiang, C. R. Xia, F. Zhao, F. L. Chen, *Electrochem. Solid State* **2009**, *12*, B91.
[37] D. Ding, B. Liu, Z. Zhu, S. Zhou, C. Xia, *Solid State Ionics* **2008**, *179*, 896.
[38] D. Ding, B. B. Liu, M. Y. Gong, X. B. Liu, C. R. Xia, *Electrochim. Acta* **2010**, *55*, 4529.
[39] M. F. Liu, D. H. Dong, R. R. Peng, J. F. Gao, J. Diwu, X. Q. Liu, G. Y. Meng, *J. Power Sources*, **2008**, *180*, 215.

Adv. Energy Mater. **2013**,
DOI: 10.1002/aenm.201200984